

JGR Solid Earth

RESEARCH ARTICLE

10.1029/2019JB018826

Special Section:

Physical Properties of Rocks, Friction and Fracturing: The Walsh Volume

Key Points:

- We investigated the electrical conductivities of Fe-free and -bearing omphacite as a function of water content at 3 GPa and 500–1300 K
- H₂O greatly enhances the EC of omphacite, while Fe facilitates EC by accelerating H diffusivity and lowering its activation enthalpy
- Fe-bearing omphacite with 0.1 wt% H₂O is a strong candidate to explain the conductivity anomalies in the Dabie-Sulu UHPM belts and Tibet

Correspondence to:

B. Zhang,
zhangbaohua@zju.edu.cn;
zhangbaohua@vip.gyig.ac.cn

Citation:

Zhang, B., Zhao, C., Ge, J., & Yoshino, T. (2019). Electrical conductivity of omphacite as a function of water content and implications for high conductivity anomalies in the Dabie-Sulu UHPM belts and Tibet. *Journal of Geophysical Research: Solid Earth*, 124, 12,523–12,536. <https://doi.org/10.1029/2019JB018826>



Received 2 OCT 2019

Accepted 19 NOV 2019

Accepted article online 26 NOV 2019

Published online 5 DEC 2019

Electrical Conductivity of Omphacite as a Function of Water Content and Implications for High Conductivity Anomalies in the Dabie-Sulu UHPM Belts and Tibet

Baohua Zhang^{1,2} , Chengcheng Zhao³, Jianhua Ge^{2,4}, and Takashi Yoshino³ 

¹Institute of Geology and Geophysics, School of Earth Sciences, Zhejiang University, Hangzhou, China, ²Key Laboratory for High-Temperature and High-Pressure Study of the Earth's Interior, Institute of Geochemistry, Chinese Academy of Sciences, Guiyang, China, ³Institute for Planetary Materials, Okayama University, Misasa, Japan, ⁴University of Chinese Academy of Sciences, Beijing, China

Abstract Magnetotelluric surveys revealed high-conductivity layers in the lower crust beneath Tibet and in the shallow part of the upper mantle relevant to continental collision extending to the Dabie-Sulu ultrahigh-pressure metamorphic (UHPM) belts of eastern China, which have been interpreted by the presence of aqueous fluids/partial melts or hydrous phases. However, these explanations are not consistent with their petrological features and seismic properties. Hydrogen-bearing omphacite could be a probable candidate to explain such high-conductivity anomalies due to its high water-partitioning coefficient versus coexisting garnet in eclogite. In this study, we investigated electrical conductivities of Fe-free and Fe-bearing omphacite as a function of water content (0.005–0.122 wt.%) at 3 GPa and 500–1300 K. Our results show that water significantly enhances the electrical conductivity of omphacite, while iron facilitates conductivity by accelerating hydrogen diffusivity and lowering its activation enthalpy. Assuming a heat flow of 70 mW/m², the high electrical anomalies observed beneath the Dabie-Sulu UHPM belts and the Tibetan Plateau can be reasonably explained by omphacite containing 0.07 wt.% water since water content higher than 0.07 wt.% in omphacite was frequently reported in naturally collected eclogite.

1. Introduction

The origin of the high-conductivity layers (HCL) (up to 0.01–1 S/m) observed by magnetotelluric (MT) and geomagnetic depth soundings in Tibet (Bai et al., 2010; Wei et al., 2001) and Dabie-Sulu ultrahigh-pressure metamorphic (UHPM) belts of eastern China (Xiao et al., 2007; Xu et al., 2016) related to continental collision has been an extensive and long-standing debate. To explain the origin of the high conductive anomalies, many possibilities such as the presence of interconnected aqueous fluids released by dehydration of hydrous minerals (e.g., Chen et al., 2018; Reynard et al., 2011; Wei et al., 2001), partial melting (Naif et al., 2013; Zhang et al., 2014), and intergranular graphite films (Frost et al., 1989; Glover, 1996) have been proposed. However, the absence of hydrous phases in the lower crustal xenoliths in 3 Ma volcanic rocks, and the observed *P* wave velocities and Poisson's ratios in the central Tibet do not match with the presence of fluid or melt-bearing rocks (Hacker et al., 2000). Wang et al. (2013) argued that graphite could significantly enhance the electrical conductivity of olivine-rich aggregates if the volume fraction of graphite exceeds ~1.6 vol%. However, it is also questioned since graphite is readily destroyed due to its high interfacial energy between silicate minerals (Yoshino & Noritake, 2011; Zhang & Yoshino, 2017) and thus cannot be maintained stably over a long geological time.

The main constituent rock in the lowermost part of thickened continental crust and subducted oceanic crust (Anderson, 2005) is eclogite, which is mainly composed of omphacite and garnet and plays a key role in mantle convection due to its relatively high density (Irifune et al., 1986; Mooney & Kaban, 2010; Xu et al., 2019). There were several studies on direct electrical conductivity measurement of natural eclogite (e.g., Bagdassarov et al., 2011; Guo et al., 2014; Laštovičková & Parchomenko, 1976), which indicated that natural eclogite failed to create the high conductive anomaly observed. Water in nominally anhydrous minerals

(NAMs) could be an alternative to raise the electrical conductivity of eclogite. Therefore, knowledge of electrical properties of eclogite is also crucial for understanding water recycling into the mantle carried by omphacite and garnet during deep subduction.

Omphacite, whose composition lies at midpoint in diopside ($\text{CaMgSi}_2\text{O}_6$)-Jadeite ($\text{NaAlSi}_2\text{O}_6$) join, is a major water host in eclogite with a H_2O partitioning coefficient as high as $D^{\text{Omp/Grt}} \approx 5\text{--}10$ (Katayama et al., 2006; Sheng et al., 2007). If the electrical conductivity of hydrogen-bearing omphacite is significantly higher than that of the coexisting garnet, then the observed HCL in stable middle-to-lower continental crust and beneath the Dabie-Sulu UHPM belts could be explained by proton conduction of omphacite. The influence of water on the electrical conductivity of natural clinopyroxene has been investigated experimentally (Wang et al., 1999; Yang et al., 2011; Yang & McCammon, 2012; Liu et al., 2019). Recently, Liu et al. (2019) measured the electrical conductivity of natural omphacite and garnet at 1 GPa and 623–1073 K whose water was incorporated by preannealing (only up to 290 ppm for omphacite and to 90 ppm for garnet). Since their omphacite was measured at narrow range of water content and fixed iron content, the effect of water and Fe (small polaron) on the electrical conductivity of omphacite is poorly constrained. To clarify the effect of water and iron on the electrical conductivity of omphacite, we measured its electrical conductivity as a function of water and iron content. Our results are of crucial importance to understand the origin of the high conductive anomalies observed beneath the Dabie-Sulu UHPM belts and Tibet. In this paper, a new explanation is proposed to account for the high conductivity anomalies exhibited.

2. Experimental Methods

Both Fe-free and Fe-bearing glasses with stoichiometric omphacite compositions were prepared from a mixture of oxides (MgO , SiO_2 , Al_2O_3 , and Fe_2O_3) and carbonates (CaCO_3 and Na_2CO_3). These two mixtures were decarbonated in a furnace at 1233 K to remove CO_2 from the powder. After that, these two kinds of calcined powders were loaded into a one-end-welded Pt tube separately, heated at 1723 K in air for 30 min and then quenched into water. For Fe-bearing omphacite glass, another 2 hr of baking at 1273 K in a gas mixing furnace at controlled oxygen fugacity close to Ni-NiO (NNO) buffered condition was adopted before quenching it into water. Electron microprobe analysis (EPMA) of these glass specimens confirmed that they were uniform with compositions of $(\text{Ca}_{0.51}\text{Mg}_{0.54}\text{Na}_{0.49}\text{Al}_{0.49}\text{Si}_{1.98}\text{O}_6)$ and $(\text{Ca}_{0.53}\text{Mg}_{0.43}\text{Fe}_{0.17}\text{Na}_{0.51}\text{Al}_{0.40}\text{Si}_{2.01}\text{O}_6)$ for Fe-free and Fe-bearing systems, respectively (Table 1), close to the stoichiometric omphacite in natural eclogite (Katayama et al., 2006; Sheng et al., 2007). The obtained glasses were then ground finely for sintering experiment.

To elucidate the effect of water content on electrical conductivity of omphacite, Fe-free and Fe-bearing omphacite aggregates with different water contents were synthesized under NNO buffered condition at 3–5 GPa, 1273 K for 2 hr in a Kawai-type multianvil press. To synthesize omphacite with high water content, glass powder was loaded into a Pt or AuPd capsule with free water and sealed by welding, while to synthesize less hydrogen-bearing omphacite aggregates, the starting powder was carefully protected from moisture before and after it was loaded into Ni (occasionally Fe) capsule. All the recovered samples were well sintered without cracks. Scanning electron microscope images showed equigranular texture with an average grain size of 3–5 μm . The sintered aggregates were cut into several pieces of ~1 mm thickness and then cylindrically cored to make disks with ~1.5-mm diameter by ultrasonic drilling machine. Thus, the reacted zone with capsule was removed, and these disks were then used for subsequent measurement.

The cell design for the conductivity measurement is shown in Figure 1. A disk-shaped sample was placed between two nickel electrodes whose surfaces were oxidized to keep oxygen fugacity near NNO buffer during measurement. Two sets of WRe_3 - WRe_{25} thermocouples were connected to Ni electrodes on both sides and insulated from graphite heater by MgO insulator. The assembled cell was dried overnight at 473 K in a vacuum furnace before conductivity measurement. Pressure was calibrated at high temperature by phase transition of albite to jadeite (2.4 GPa and 1173 K) and by conductivity jump due to phase transition of fayalite ($\alpha \rightarrow \gamma$ at 5.6 GPa and 1373 K, 6.6 GPa and 1573 K) (Zhang & Yoshino, 2016). After compressing to 3 GPa in a Kawai-type multianvil apparatus, the adhesive water in the surrounding materials was purged by preheating sample at 500 or 800 K for more than 2 hr, with monitoring of the sample resistance. Complex impedance spectra were acquired using a Solartron 1260 Impedance/Gain-Phase Analyzer (combined with a Solartron 1296 Interface when the sample resistance was higher than $\text{M}\Omega$) over frequencies from 10^6 to

Table 1
Chemical Compositions of the Starting Material and the Run Products

| | Startingmaterial ^a (n = 7) | Startingmaterial ^b (n = 7) | 5 K3261 ^c (n = 5) | 5 K3262 ^c (n = 5) | 5 K3263 ^c (n = 5) | 5 K3264 ^c (n = 5) | 5 K3265 ^c (n = 5) | 5 K3376 ^c (n = 6) | 5 K3379 ^c (n = 5) |
|--------------------------------|--|--|---------------------------------|---------------------------------|---------------------------------|---------------------------------|---------------------------------|---------------------------------|---------------------------------|
| SiO ₂ | 55.40(0.26) | 56.35(0.34) | 55.31(0.36) | 56.51 (0.33) | 56.26(0.29) | 55.92(0.34) | 57.05(0.32) | 61.19(0.42) | 56.32(0.38) |
| Al ₂ O ₃ | 9.31(0.14) | 11.76(0.16) | 8.93(0.13) | 11.83 (0.20) | 8.40(0.17) | 9.21 (0.15) | 11.29 (0.22) | 11.29(0.14) | 9.43 (0.25) |
| FeO ^d | 5.71 (0.26) | 0 | 5.74 (0.15) | 0 | 5.64 (0.15) | 5.81 (0.12) | 0 | 0 | 6.51 (0.17) |
| MgO | 8.01 (0.12) | 10.39 (0.17) | 8.65 (0.14) | 10.68 (0.16) | 7.74 (0.10) | 8.18 (0.15) | 9.10 (0.13) | 8.13 (0.09) | 7.31 (0.15) |
| CaO | 13.72 (0.20) | 13.64 (0.19) | 14.22 (0.20) | 13.53 (0.21) | 13.29 (0.25) | 13.57 (0.17) | 12.91 (0.21) | 12.23 (0.23) | 12.99 (0.18) |
| Na ₂ O | 7.21 (0.11) | 7.23 (0.09) | 7.18 (0.13) | 7.05 (0.14) | 6.97 (0.12) | 6.89 (0.14) | 6.83 (0.17) | 7.11 (0.16) | 7.42 (0.08) |
| Total | 99.36 (0.32) | 99.37 (0.26) | 100.03 (0.14) | 99.59 (0.25) | 98.30 (0.44) | 99.58 (0.32) | 97.18 (0.56) | 99.95 (0.16) | 99.98 (0.20) |
| O = 24 | | | | | | | | | |
| Si | 8.03 (0.12) | 7.9 3(0.10) | 8.04 (0.12) | 8.04 (0.08) | 8.11 (0.11) | 8.13 (0.09) | 8.15 (0.13) | 8.42 (0.11) | 8.10 (0.13) |
| Al | 1.59 (0.09) | 1.95 (0.06) | 1.39 (0.07) | 1.95 (0.08) | 1.52 (0.07) | 1.40 (0.06) | 1.90 (0.05) | 1.83 (0.08) | 1.60 (0.07) |
| Fe | 0.69 (0.06) | 0 | 0.74 (0.04) | 0 | 0.70 (0.04) | 0.72 (0.05) | 0 | 0 | 0.78 (0.03) |
| Mg | 1.73 (0.05) | 2.18 (0.10) | 1.88 (0.09) | 2.02 (0.06) | 1.68 (0.05) | 1.81 (0.05) | 1.94 (0.07) | 1.67 (0.04) | 1.57 (0.05) |
| Ca | 2.13 (0.05) | 2.06 (0.08) | 2.21 (0.06) | 2.03 (0.07) | 2.08 (0.09) | 2.15 (0.05) | 1.98 (0.06) | 1.80 (0.07) | 2.00 (0.08) |
| Na | 2.03 (0.04) | 1.97 (0.05) | 1.94 (0.05) | 1.91 (0.03) | 1.97 (0.04) | 1.92 (0.04) | 1.89 (0.05) | 1.90 (0.06) | 2.07 (0.07) |
| Total | 16.20 (0.15) | 16.09 (0.14) | 16.20 (0.16) | 15.95 (0.13) | 16.06 (0.14) | 16.13 (0.17) | 15.86 (0.12) | 15.62 (0.11) | 16.12 (0.18) |

Note. The chemical compositions of omphacite were measured by the electron probe microanalyzer under the operating condition of 15 kV and 10 nA. ^aChemical composition of Fe-bearing starting material was determined from fragment of quenched glass, which was used to synthesize Fe-bearing omphacite sample. ^bChemical composition of Fe-free starting material was determined from fragment of quenched glass, which was used to synthesize Fe-free omphacite sample. ^cChemical composition of omphacite were determined after the conductivity measurements. ^dIn FeO it is assumed that all iron is ferrous iron.

10⁻¹ Hz under alternating current (AC) voltage with an amplitude of 1 V. In order to check the reproducibility of conductivity measurement (Yoshino, 2010), several heating-cooling cycles were performed. Within each cycle, impedance spectra were obtained at a temperature step of 50 or 100 K. For omphacite with the highest water content, conductivity measurement was performed up to 1200 K to suppress sample dehydration (Yoshino et al., 2006; Zhang et al., 2012; Zhao & Yoshino, 2016), while for sample with relatively low water content, conductivity was measured up to 1300 K (Table 2). Sample conductivity (σ) was calculated from sample resistance R (Ω), sample thickness L (m), and cross-sectional area of sample S (m²) after conductivity measurements through the relation $\sigma = L/(R \times S)$. Experimental errors on the calculated conductivity were estimated to be less than 5%, which arose mainly from the change in the sample dimension (L/S) during compression and heating.

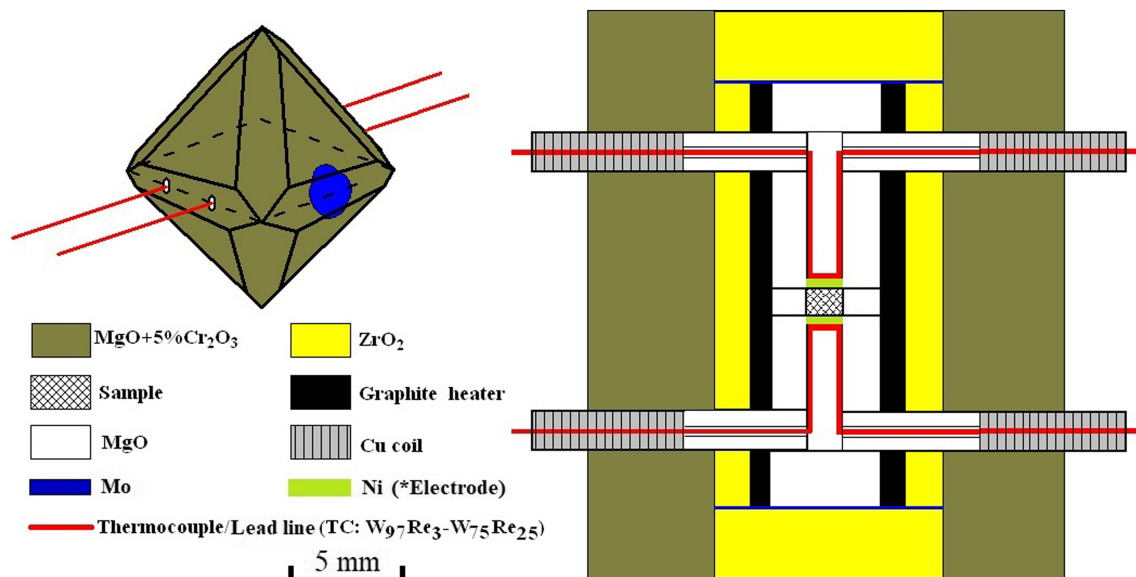


Figure 1. Schematic cross section of high-pressure cell assembly for electrical conductivity measurements in the Kawai-type multianvil press.

Table 2
Summary of Experimental Runs

| Run No. | FeO ^a (wt.%) | H ₂ O ^b (wt.%) | H ₂ O ^c (wt.%) | Length (mm) | Radius (mm) | T (K) | σ ₀ (S/m) | ΔH (eV) |
|---------|-------------------------|--------------------------------------|--------------------------------------|-----------------------|-----------------------|----------|----------------------|----------|
| 5 K3262 | 0 | 0.123 (11) | 0.122 (8) | 0.98 (4) | 1.42 (3) | 500–1200 | 47.1 (9) | 0.85 (1) |
| 5 K3265 | 0 | 0.036 (4) | 0.034 (3) | 0.96 (3) | 1.40 (5) | 600–1300 | 33.7 (12) | 0.99 (3) |
| 5 K3376 | 0 | 0.004 (3) | 0.005 (5) | 0.54 (2) ^d | 1.95 (3) ^d | 600–1200 | 7.64 (21) | 1.01 (2) |
| 5 K3261 | 5.74 (12) | 0.046 (4) | 0.044 (4) | 0.95 (5) | 1.47 (2) | 500–1200 | 20.2 (4) | 0.68 (1) |
| 5 K3263 | 5.64 (16) | 0.057 (6) | 0.052 (6) | 0.98 (2) | 1.44 (3) | 500–1200 | 28.5 (2) | 0.76 (1) |
| 5 K3264 | 5.81 (21) | 0.054 (5) | 0.055 (5) | 0.96 (3) | 1.41 (2) | 500–1300 | 130.8(30) | 0.66 (2) |
| 5 K3379 | 6.51 (25) | 0.007 (5) | 0.008 (6) | 0.97 (2) | 1.36 (5) | 550–1200 | 4.42 (12) | 0.72 (1) |

Note. All conductivity measurement experiments were performed at 3 GPa. The recovered run products show very weak distortions and changes in dimension (initial radius, ~1.0 mm; initial length, ~1.5 mm). Numbers in parentheses are the errors by the nonlinear least squares fitting using equation (1) (1 sigma standard deviation).

^aFeO wt.% in omphacite after the conductivity measurements determined by EPMA analysis. ^bH₂O wt.% in omphacite before the conductivity measurements determined by FT-IR analysis using Paterson (1982) calibration. ^cH₂O wt.% in omphacite after the conductivity measurements determined by FT-IR analysis using Paterson (1982) calibration. ^dThe initial sample dimension (radius, ~0.6 mm; length, ~2.0 mm) for run 5 K3376.

After conductivity measurement, the major element composition was determined by EPMA (Table 1) and the phase in the recovered sample was confirmed to be omphacite by a micro-focused X-ray diffraction (XRD). To determine water content, samples before and after conductivity experiments were double polished to ~150-μm thickness and measured by Fourier-transformation infrared (FT-IR) spectroscopy using Jasco FTIR-6200 Equipper with IRT-7000 infrared microscope, with 50 × 50 μm aperture size large enough to incorporate dozens of grains. At least five different spots were measured for each sample using unpolarized light. Water content in samples was calculated using the equation given by Paterson (1982), with an integration range of 2,800–3,700 cm⁻¹. Figure 2 shows the representative IR spectra of omphacite aggregates before and after electrical conductivity measurement. Three groups of OH-stretching bands can be distinguished: (1) 3,620–3,640, (2) 3,530–3,564, and (3) 3,440–3,460 cm⁻¹ irrespective of water content. The bands of Groups (2) and (3) are usually stronger whereas those of Group (1) are very weak. This feature is consistent with previous observation by Koch-Müller et al. (2004), while differing from those reported by Katayama et al. (2006) which showed extremely intense band of Group (1). Before and after conductivity measurement, similar IR spectra and near the same water content were obtained (Table 1 and Figure 2), suggesting no obvious water loss occurred during conductivity experiment.

3. Experimental Results

Figure 3 shows the representative complex impedance spectra acquired for Fe-free and Fe-bearing omphacite samples at 3 GPa and different temperatures. All the measured impedance spectra display semicircular arc at high frequencies, with a tiny tail at frequencies lower than 100 Hz occasionally, possibly indicating that the resistance increases during the conductivity measurement. Sample resistance was determined using the fitting result from high-frequency portion of the spectrum. Figure 4 shows a typical example of conductivity measurement in three heating-cooling cycles between 500 and 1200 K for water-doped sample (5 K3261). In general, during successive heating-cooling cycles conductivity paths become straighter and steeper (Figure 4), demonstrating excellent reproducibility. This reproducibility shows that the sample did not undergo oxidation or reduction during the conductivity measurement. The straight line suggests that the conduction mechanism did not change in this temperature range and hydrogen was kept as structured water during the conductivity measurement (Figure 2 and Table 2). Conductivity values obtained from the last path were used for analysis.

Figure 5 shows the electrical conductivity obtained for omphacite with various H₂O and iron contents in Arrhenius plot. Log conductivity of sample exhibits a linear relationship with reciprocal temperature and can be expressed by the Arrhenius equation:

$$\sigma = \sigma_0 \exp\left(-\frac{\Delta H}{k_B T}\right) \quad (1)$$

where σ₀ is the preexponential factor, ΔH is the activation enthalpy (eV), k_B is the Boltzmann constant, and T is the absolute temperature. The preexponential factor and the activation enthalpy (ΔH) for each sample

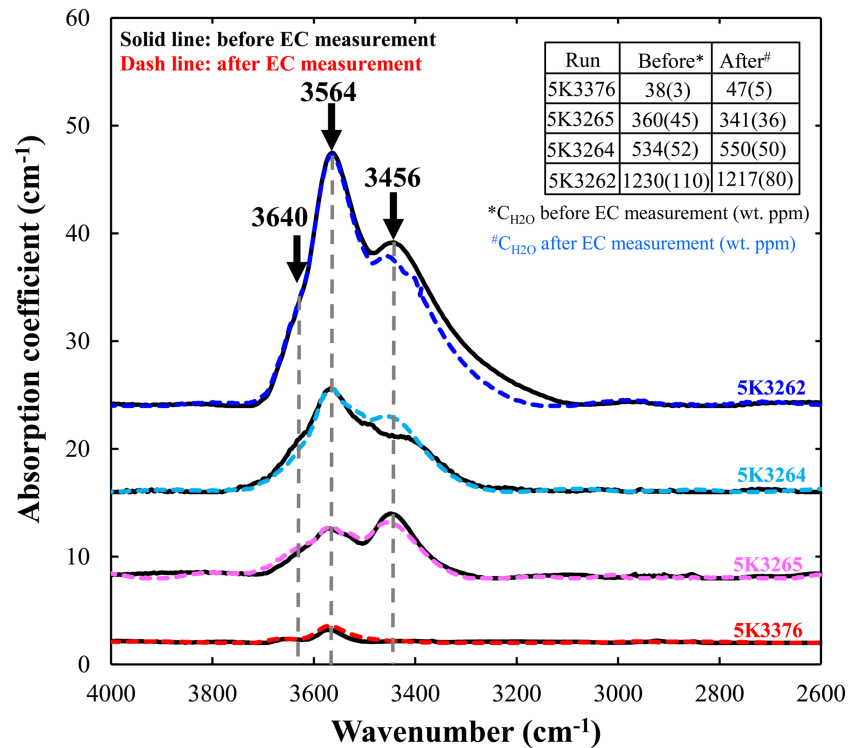


Figure 2. Unpolarized FT-IR spectra of omphacite aggregates before and after the conductivity measurements.

are summarized in Table 2. The conductivity of hydrous Fe-free omphacite sample increases 1 order of magnitude when H₂O content is increased from 0.005 to 0.034 and from 0.034 to 0.122 wt.%, respectively, while the activation enthalpy decreases from 0.99 to 0.85 eV (Figure 5). A similar trend is found in Fe-bearing omphacite, although those three samples with small variation of H₂O contents show almost identical electrical conductivities and activation enthalpies. Fe-bearing sample with low water content (~0.008 wt.%) shows one log unit higher conductivity than that of the Fe-free one with similar water content (~0.005 wt.% in Figure 5).

In order to quantify the effect of H₂O and Fe contents on electrical conductivity and understand conduction mechanisms, all experimental data are fitted by the following equation:

$$\sigma = \sigma_0 X_{\text{Fe}}^n C_{\text{H}_2\text{O}}^r \exp\left(-\frac{\Delta E_0 - \alpha X_{\text{Fe}} - \beta C_{\text{H}_2\text{O}}^{1/3}}{k_B T}\right) \quad (2)$$

where X_{Fe} is the mole fraction of iron ($X_{\text{Fe}} = \text{Fe}/(\text{Fe} + \text{Mg})$); $C_{\text{H}_2\text{O}}$ is the water content in weight percent; ΔE_0 is the activation energy; and n , r , α , and β are constants. The linear least squares regression of the global data set to equation (2) yielded $\sigma_0 = 1,483$ (260) S/m, $n = 0.09$ (3), $r = 1.10$ (10), $\Delta E_0 = 1.05$ (3) eV, $\alpha = 0.71$ (5) eV, and $\beta = 0.38$ (7) eV. The fitting result reproduces our experimental data well (Figure 5).

4. Discussion

4.1. Charge Transport Mechanisms

In the present study, electrical conductivity of hydrous Fe-free omphacite increases with increasing H₂O content, while the activation enthalpy decreases (Figure 5). There is a linear relation between electrical conductivity and reciprocal temperature in hydrous Fe-free omphacite, implying a single thermally activated conduction mechanism. The strong H₂O content dependences of conductivity and activation enthalpy are comparable with that in other NAMs (e.g., olivine: Yoshino et al., 2006; Poe et al., 2010; orthopyroxene: Zhang et al., 2012; clinopyroxene: Zhao & Yoshino, 2016), suggesting that proton conduction should be

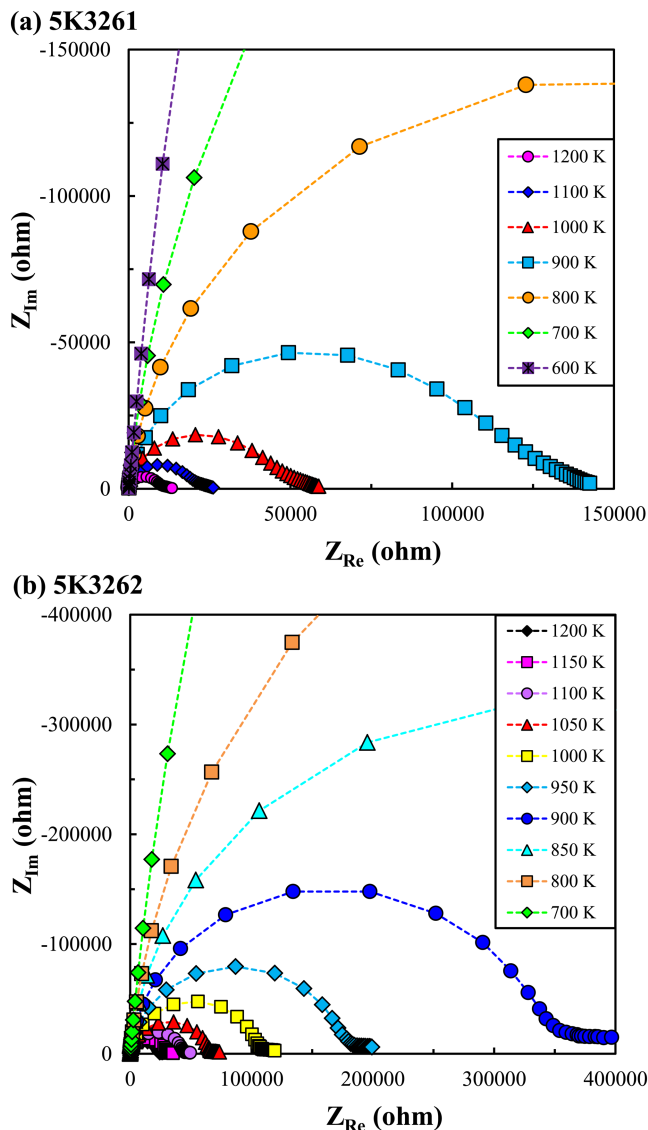


Figure 3. Representative complex impedance spectra of Fe-bearing (a) and Fe-free (b) omphacite aggregates at frequencies ranging from 1 MHz to 0.1 Hz at the temperatures indicated. Dashed lines indicate the fit results by R-CPE (resistance-constant phase element) parallel circuit.

the dominant charge transport mechanism. The significant H₂O-enhanced electrical conductivity could be attributed to the increased incorporation of hydrogen in the crystal structure of omphacite. Three IR spectra bands are identified (Figure 2), denoting different hydrogen positions. Group (1) near 3,640 cm⁻¹ is supposed to be related with Si vacancy or other tetrahedral defects, Group (2) near 3,564 cm⁻¹ to the substitution of Al³⁺ with Si⁴⁺ expressed as Al³⁺ + H⁺ → Si⁴⁺, and Group (3) near 3,456 cm⁻¹ to cation vacancy in M2 site due to Al³⁺ + H⁺ → 2 Mg²⁺ (Koch-Müller et al., 2004; Smyth et al., 1991). However, the IR spectra of Group (1) near 3,640 cm⁻¹ are not obvious in Figure 2, which suggests that the Si site may not be a major host for hydrogen. As hydrogen concentration increases systematically, a decrease of distance to the nearest proton can facilitate proton hopping, leading to the decrease of activation enthalpy.

For Fe-bearing omphacite, the conductivity is more than 1 order of magnitude higher than that of the Fe-free one with the same water content. Activation enthalpy of the Fe-bearing omphacite is lower (Figure 5), which suggests that Fe has large influence on its conductive behavior. Small polaron is expected to be a major charge carrier, but the exact effect cannot be quantified due to lack of data on dry Fe-bearing sample. Although Fe content varies little in Fe-bearing omphacite, the increase of conductivity and decrease of activation enthalpy with increasing X_{Fe} found in this study (Table 2) are quite similar to those observed in olivine (Omura et al., 1989; Yoshino et al., 2012), ringwoodite (Yoshino & Katsura, 2009), and orthopyroxene (Zhang & Yoshino, 2016), implying that conductivity in a hydrous Fe-bearing sample includes effects of both Fe and water. Thus, the bulk conductivity of omphacite includes the contribution from conduction by both small polarons and protons. The joining of Fe makes the movement of hydrogen easier by lowering its activation enthalpy and faster by increasing its diffusivity. When comparing the proton conduction between Fe-free and Fe-bearing samples with the same water content, the electrical conductivity of hydrous Fe-bearing omphacite is at least 1 order of magnitude higher than that of the Fe-free one (Figure 5). This observation suggests that, besides proton conduction, small polaron conduction should have a large contribution to the bulk conductivity of hydrous Fe-bearing omphacite. Their IR spectra (Figure 2) imply that hydrogen incorporation positions in Fe-bearing omphacite are basically the same with those in the Fe-free one and support that Fe serves as a modifier during conduction of hydrogen-bearing omphacite. In addition to the substitution mechanisms mentioned above, the addition of Fe might

substitute a fraction of Al in Si or Mg site or both and result in Fe³⁺ + H⁺ → Si⁴⁺ and Fe³⁺ + H⁺ → 2 Mg²⁺. The larger diameter of Fe³⁺ enlarges and distorts the original lattice sites holding Al³⁺, which leads to weaker bonding of hydrogen and therefore smaller activation enthalpy. Assuming diffusion coefficient of hydrogen in omphacite is similar to that (1.8 × 10⁻¹² m²/s at 850 °C and 6.5 × 10⁻¹² m²/s at 950 °C) in clinopyroxene reported by Xia et al. (2000), the diffusion distance (*d*) of hydrogen in omphacite is estimated to be 0.2–0.5 mm within the experimental duration (*t*~12 h) derived from the relation $d \approx (D \times t)^{1/2}$. This length scale indicates that hydrogen does not diffuse out of omphacite during the experimental duration. It is obvious that water can significantly enhance the electrical conductivity of omphacite.

4.2. Comparison With Previous Studies

Figure 6 shows a comparison of electrical conductivity of hydrous Fe-bearing omphacite in the present study with some previous studies. Huebner and Voigt (1988) reported the electrical conductivity of two natural single crystals of diopside at reducing conditions. They found that the electrical conductivity of Brazil diopside

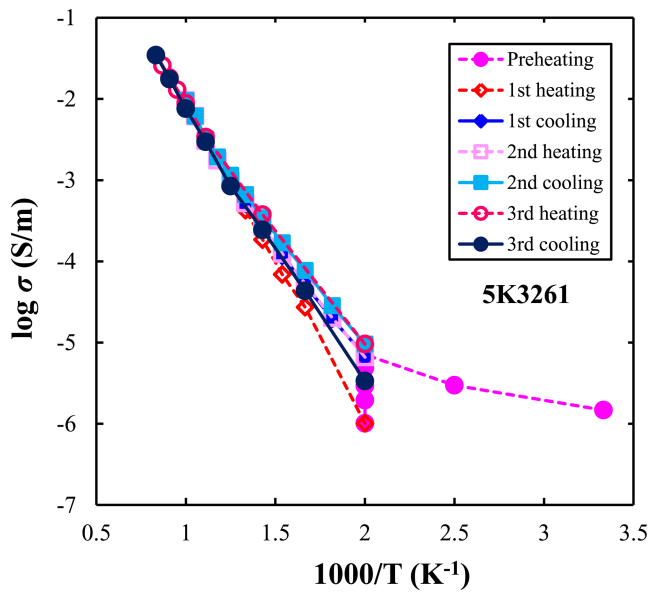


Figure 4. Electrical conductivity of hydrous Fe-bearing omphacite (5 K3261) as a function of reciprocal temperature along repeated heating-cooling cycles. Different symbols and colors indicate different heating and cooling cycles.

with higher Fe content ($Mg\# = 88$) is higher than that of DK7 diopside with lower Fe content ($Mg\# = 97$), and the activation enthalpy of Brazil diopside (~ 0.98 eV) is lower than that of DK7 diopside (~ 2.0 eV). Wang et al. (1999) investigated the effect of hydrogen on the electrical conductivity of three diopsides with almost the same Fe content ($Mg\# \approx 97$) from India, Sri-Lanka, and Russia. The Sri-Lanka diopside, which has the lowest Fe content but the highest H_2O content, shows a surprisingly high conductivity compared to the other two crystals (Russia and India diopsides). They suggested that the predominant charge carriers in the Sri-Lanka diopside are protons, and the enhancement of electrical conductivity is attributed to the dissolution of hydrogen which may increase the concentration and/or mobility of the charged intrinsic defects associated with H^+ or OH^- . Liu et al. (2019) reported the electrical conductivity of natural omphacite at 1 GPa and 623–1073 K with preannealed water-bearing sample (up to 290 ppm). Their results showed that activation enthalpy (~ 0.85 eV) is nearly independent of water content. They concluded that the conduction in omphacite is dominated by proton, and the conductivity increases linearly with water content. As shown in Figure 6, our conductivity data ($Mg\# = 67\text{--}73$) agree well with the results reported by Liu et al. (2019) ($Mg\# = 78$) while much higher than those of clinopyroxene in fertile peridotite (Zhao & Yoshino, 2016) ($Mg\# = 92$) and lower than those of clinopyroxene originated from the lower crust (Yang, 2012; Yang et al., 2011; Yang & Heidelbach, 2012) ($Mg\# = 72$). For hopping conduction,

all data set on nominally dry clinopyroxene display a strong positive dependence of electrical conductivity on iron content. Conductivity increases with increasing total iron content while activation enthalpy decreases accordingly. This trend has been observed in other iron-bearing minerals (Omura et al., 1989; Yoshino et al., 2012; Yoshino & Katsura, 2009; Zhang & Yoshino, 2016).

With increasing water content, the conductivities obtained in this study are higher than those reported by Liu et al. (2019) at the same water content, T and f_{O_2} conditions, and ~ 1.5 orders of magnitude higher than

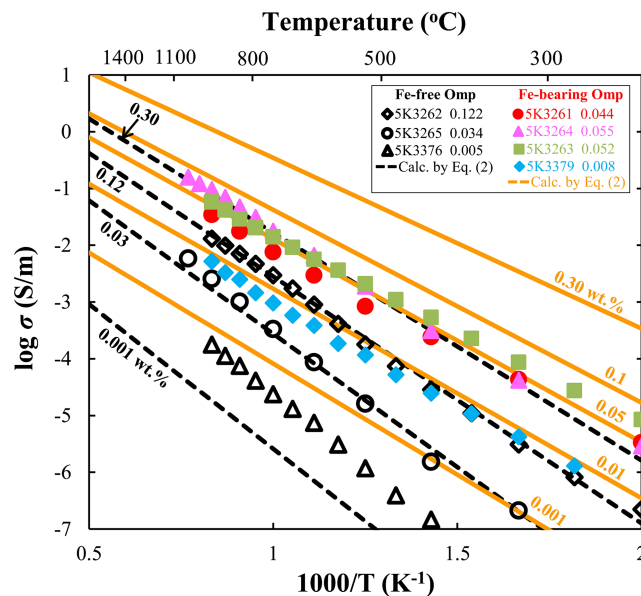


Figure 5. Electrical conductivities of omphacite with various amounts of water as a function of reciprocal temperature at 3 GPa. Open and closed symbols represent raw data for Fe-free and Fe-bearing omphacite, respectively. The numbers denote the water content (in wt.%). Dashed black and solid thick orange lines indicate fitting results of equation (2) for Fe-free and Fe-bearing omphacite as a function of water content.

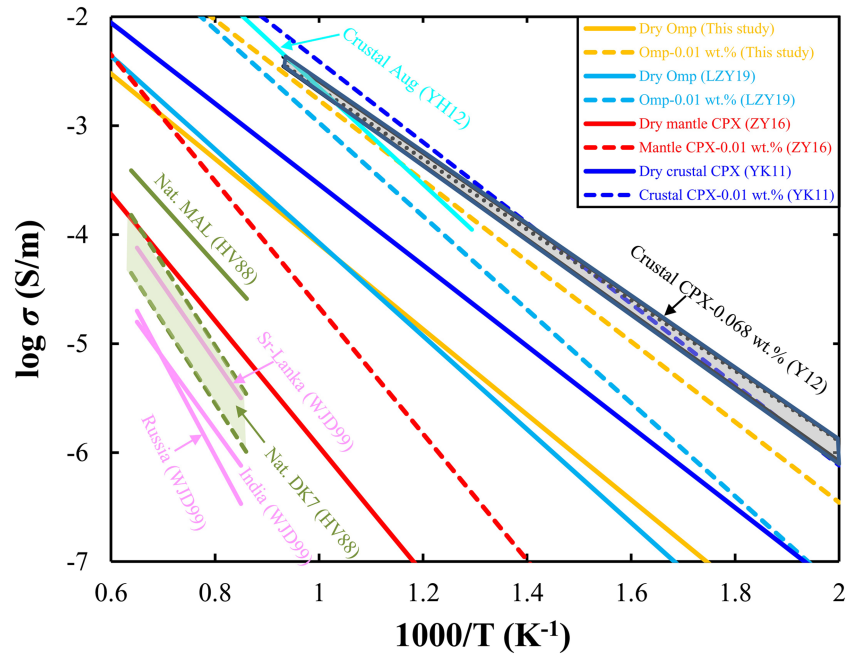


Figure 6. Composition of the electrical conductivity of omphacite (the orange lines from this study) with previous studies. Data source: HV88—Huebner and Voigt (1988); WJD99—Wang et al. (1999); YK11—Yang et al. (2011); Y12—Yang (2012); YH12—Yang and Heidelberg (2012); ZY16—Zhao and Yoshino (2016); LZY19—Liu et al. (2019).

those of mantle clinopyroxene measured by Zhao and Yoshino (2016). It is worth noting that the water content exponent of $r \sim 1.1$ obtained in this study is exactly the same as that in omphacite derived from Liu et al. (2019) and in crustal clinopyroxene from Yang et al. (2011) while smaller than that ($r = 1.28$) in mantle clinopyroxene from Zhao and Yoshino (2016). The activation enthalpy determined in this study (0.68–0.76 eV in Table 2) is smaller than that of Liu et al. (2019) (~0.85 eV) and those of mantle clinopyroxene from Zhao and Yoshino (2016) (0.70–1.01 eV). Liu et al. (2019) argued that the activation enthalpy is nearly independent of

water content. The present investigation demonstrated that the activation enthalpy slightly decreases with increasing water content (Table 2), which is consistent with observation in mantle clinopyroxene (Zhao & Yoshino, 2016). The large discrepancies on conductivity and activation enthalpy for hydrous Fe-bearing clinopyroxene, especially for proton conduction, could be explained by the difference in total iron content between crustal clinopyroxene (Liu et al., 2019; Yang, 2012; Yang et al., 2011; Yang & Heidelberg, 2012) and mantle clinopyroxene (Zhao & Yoshino, 2016), while the extremely high conductivity (Figure 6) reported by Yang (2012) and Yang and Heidelberg (2012) may be due to higher Fe^{3+} content in their samples. As discussed above, iron facilitates conductivity by accelerating hydrogen diffusivity and lowering its activation enthalpy, suggesting that the bulk conductivity of hydrous iron-bearing omphacite is greatly affected not only by hydrogen concentration but also by iron content.

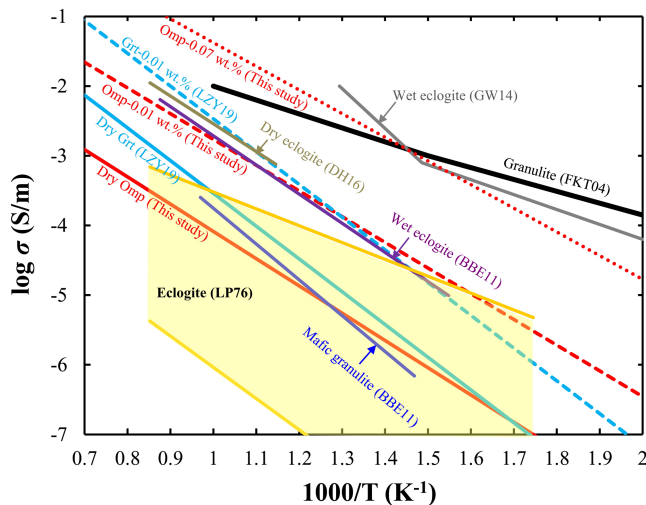


Figure 7. Composition of the electrical conductivity of omphacite (the red lines from this study) with garnet, granulite, and eclogite. Data source: LP76—Laštovičková and Parchomenko (1976); FKT04—Fuji-ta et al. (2004); BBE11—Bagdassarov et al. (2011); GW14—Guo et al. (2014); DH16—Dai et al. (2016); LZY19—Liu et al. (2019).

4.3. Comparison of Conductivity of Granulite and Eclogite

Electrical conductivity of eclogite largely depends on the electrical conductivity of its major minerals and corresponding volume fractions. According to the present experiment, the electrical conductivity of dry omphacite is lower than that of dry garnet measured by Liu et al. (2019) at high temperatures (>600 K). The same trend is also observed in hydrous cases (Figure 7). Laštovičková and Parchomenko (1976) first

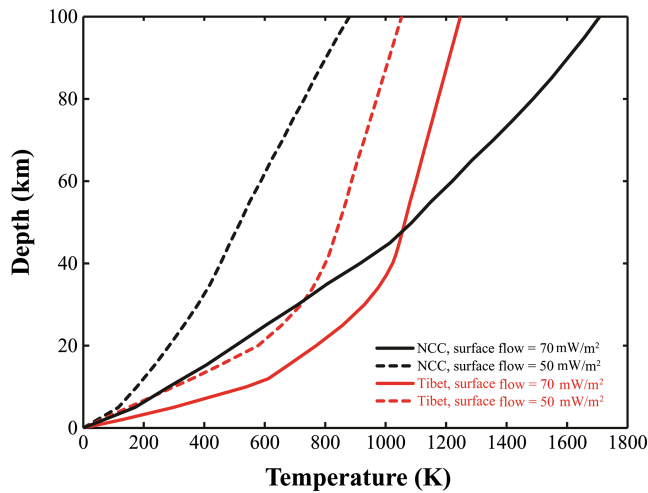


Figure 8. Depth-temperature relations of the North China Craton (NCC) (Miao et al., 2014) and the Tibetan Plateau with different surface heat flow (Hu et al., 2000).

studied the electrical conductivity of eight species of eclogites from the Bohemian Massif at pressures up to 2.0 GPa using direct current (DC) and single-frequency AC technique. They found that the electrical conductivity of eclogite is strongly affected by the content of symplectite minerals (e.g., intergrowths of amphibole, plagioclase, and diopside). Bagdassarov et al. (2011) reported the electrical conductivity of the At-Bashi eclogite at pressures of 0.8–2.5 GPa by impedance spectra measurement. Although no information of water content was provided, their conductivities and activation enthalpy (0.83 eV) are comparable to those of dry Dabie-Sulu eclogite measured by Dai et al. (2016) but much lower than that of hydrous Tibet eclogite reported by Guo et al. (2014). This discrepancy is mainly attributed to the large difference in their mineralogical composition and total Fe and H₂O content. For example, the Tibet eclogite (Guo et al., 2014) contains ~40 vol% garnet, ~30 vol% omphacite, ~25 vol% glaucophane, and ~5 vol% rutile and quartz. The iron contents in garnet and omphacite are 29.16 and 6.67 wt.%, respectively. The bulk water in the Tibet eclogite is 0.63 wt.%. In contrast, the mineralogical and iron contents in the At-Bashi eclogite (~25 vol% garnet, ~60 vol% omphacite and ~10 vol% glaucophane) are similar to those in dry Dabie-

Sulu eclogite (~41 vol% garnet and ~58 vol% omphacite, <1 vol% accessory minerals). The iron content in omphacite from At-Bashi eclogite ($X_{\text{Fe}} = 0.22$) (Bagdassarov et al., 2011) is almost the same as that in Dabie-Sulu eclogite ($X_{\text{Fe}} = 0.25$) (Dai et al., 2016), whereas the iron content in garnet of the former ($X_{\text{Fe}} = 0.79$) is a little lower than that of the latter ($X_{\text{Fe}} = 0.91$).

On the other hand, the electrical conductivity of eclogite is also compared with that of granulite in Figure 7. Fuji-ta et al. (2004) measured the electrical conductivity of granulite under middle- to lower-crustal pressure-temperature conditions. Their conductivity is close to that of hydrous eclogite (Guo et al., 2014), while much higher than those of mafic granulite (Bagdassarov et al., 2011) and eclogites (Bagdassarov et al., 2011; Dai et al., 2016; Laštovičková & Parchomenko, 1976). The electrical conductivity of mafic granulite (Bagdassarov et al., 2011) is in agreement with those of dry omphacite (this study) and garnet (Liu et al., 2019) and falls within the results presented by Laštovičková and Parchomenko (1976). Based on these experimental investigations, the conductivity discrepancies of granulite between Fuji-ta et al. (2004) and Bagdassarov et al. (2011) are mainly caused by either more abundant garnet or higher water content in the former. However, further experimental work is required to clarify this issue, especially for water effect on conductivity.

4.4. Geophysical Implications

Combination of laboratory conductivity data with petrological models can provide important constraint on the interpretation of results from MT soundings. To better explain the high conductive anomalies in the Dabie-Sulu UHPM belts and the Tibetan Plateau, we construct conductivity-depth profiles based on Fe-bearing omphacite from this study and garnet from Liu et al. (2019) using two different sets of geotherm with heat flows of 50 and 70 mW/m² (Hu et al., 2000; Miao et al., 2014) (Figure 8). The effective medium model (Landauer, 1952) was used to calculate conductivities of two coexisting phases:

$$\sigma_{\text{EM}} = \frac{1}{4} \left\{ (3f_1 - 1)\sigma_1 + (3f_2 - 1)\sigma_2 + [(3f_1 - 1)\sigma_1 + (3f_2 - 1)\sigma_2^2 + 8\sigma_1\sigma_2]^{\frac{1}{2}} \right\} \quad (3)$$

where σ_1 and σ_2 are the conductivities of two coexisting phases, and f_1 and f_2 are their corresponding volume fractions. Although accessory minerals (i.e., phengite, rutile, diamond, quartz/coesite, etc.) are found in eclogites, they are difficult to form interconnected networks because of their small amount (less than 20% or less). Thus, the isolated accessory minerals in the matrix contribute little to the bulk conductivity of eclogite. To maximize the omphacite contribution to bulk conductivity, eclogite is assumed to be the major rock in the lowermost part of thickened continental crust, which is composed of omphacite and garnet with various volume ratio from 30:70, 50:50 to 70:30. Water partitioning coefficient is assumed to be $D_{\text{H}_2\text{O}}^{\text{Omp/Grt}} = 5$ (Katayama et al., 2006; Sheng et al., 2007), independent of pressure, temperature, and

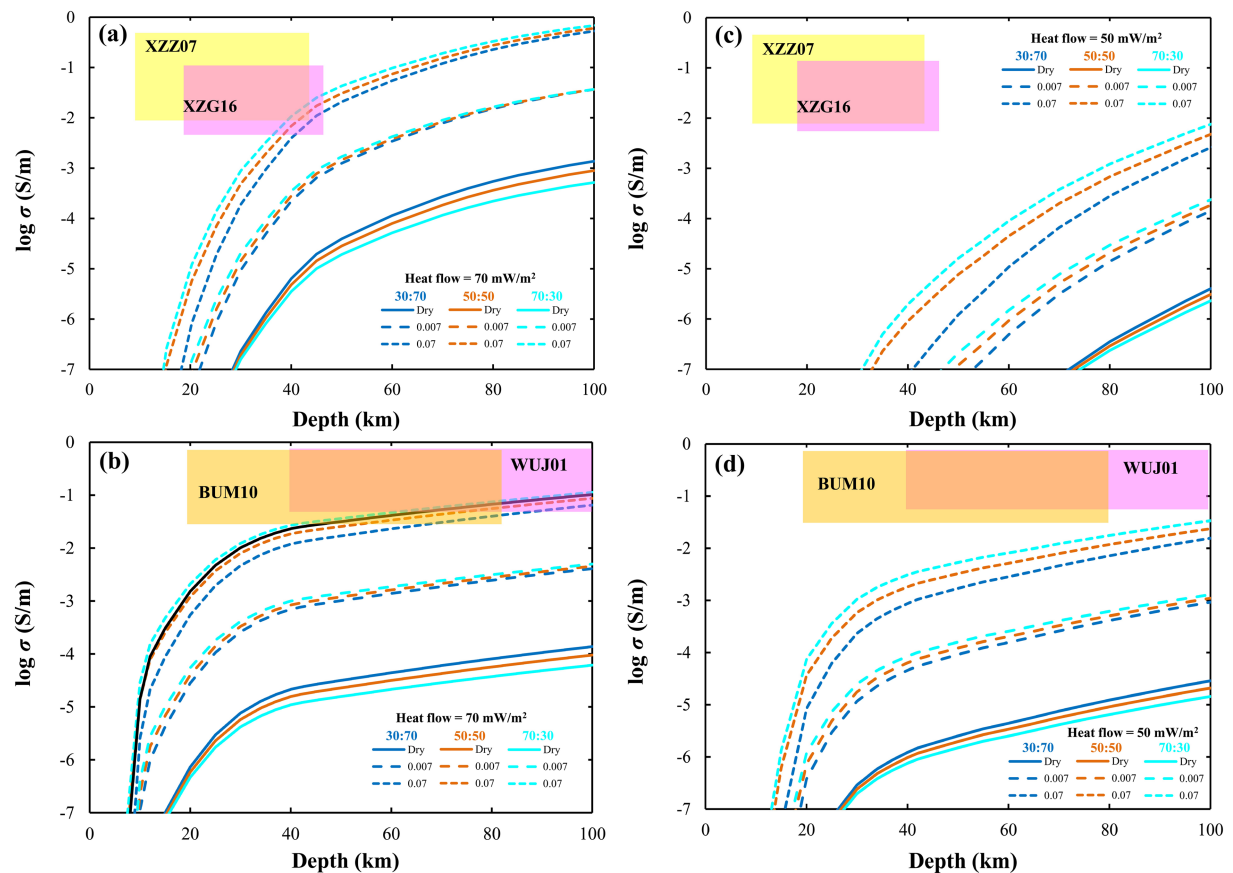


Figure 9. Laboratory-based conductivity-depth profiles as a function of water contents and mineral volume fractions compared with the previous geophysical models. The yellow and pink areas represent geophysically observed high conductivity anomalies under the Dabie-Sulu UHPM belts of eastern China (XZZ07: Xiao et al., 2007; XZG16: Xu et al., 2016) (a) and beneath the Tibetan Plateau (WUJ01: Wei et al., 2001; BUM10: Bai et al., 2010) (b), respectively, using surface heat flow of 70 mW/m^2 . In the same region, (c) and (d) were calculated from a lower surface heat flow of 50 mW/m^2 . Note that solid, dashed, and short dashed lines denote dry and 0.01 and 0.1 wt.% H_2O . Blue, orange, and cyan colors stand for ratio of mineral volume fractions omphacite:garnet = 30:70, 50:50, 70:30, respectively.

chemical composition. Water content in omphacite was set to be 0.007 and 0.07 wt.% during calculating conductivity in terms of equation (2) and in garnet to be 0.0014 and 0.014 wt.%. The lower bound of electrical conductivity is defined by assuming eclogite to be dry (1 wt. ppm for omphacite and 0 wt. ppm for garnet). As shown in Figure 6, the measured conductivities of dry omphacite between this study (3 GPa) and Liu et al. (2019) (1 GPa) are nearly identical, suggesting a negligible effect of pressure on conductivity. In addition, Yang and Heidelbach (2012) revealed that the electrical conductivity of clinopyroxene is independent of grain size. To simplify our model, effects of pressure, grain size, and additional phases on the bulk rock conductivity were not considered. Two sets of typical geotherm with heat flows of 50 and 70 mW/m^2 (Hu et al., 2000) were adopted to calculate the temperature distribution along with depth in different tectonic active zones (i.e., the Dabie-Sulu UHPM belts and the Tibetan Plateau) since conductivities are highly dependent on geothermal structures. The geotherm structure under the Dabie-Sulu UHPM belts of eastern China and the Tibetan Plateau was estimated from surface heat flow and thermal properties of the main rocks in the lithospheric mantle (Miao et al., 2014). In the Dabie-Sulu UHPM belts, the mean value for the surface flow is around 50 mW/m^2 , and the upper bound is about 70 mW/m^2 , while 50 and 70 mW/m^2 correspond to the lower bound and the mean value in the Tibetan Plateau (Hu et al., 2000). Oxygen fugacity is assumed to be Ni-NiO buffered because subducted slabs are usually oxidized (Frost & McCammon, 2008). Owing to the observation that conductivity difference in eclogite between NNO and QFM buffered conditions at 2 GPa is only 0.1 log units (Dai et al., 2016), the influence of oxygen fugacity in this calculation was not considered. Figure 9a illustrates the conductivity-depth profiles for the Dabie-Sulu UHPM belts of eastern China with a relatively high heat flow

of 70 mW/m^2 corresponding to its upper bound. It can be clearly seen that the electrical conductivity of dry eclogite cannot explain the high conductive anomalies regardless of heat flow and mineral volume fraction (Figure 9), which agrees with previous result reported by Dai et al. (2016). However, as water content in Fe-bearing omphacite increases from 0.007 to 0.07 wt.% (in garnet from 0.0014 to 0.014 wt.%), the conductivity increases by more than 1 order of magnitude. Therefore, the HCL observed beneath the Dabie-Sulu UHPM belts of eastern China ($\sim 10^{-2.2}$ – $10^{-0.5}$ S/m) (Xiao et al., 2007; Xu et al., 2016) can be reasonably explained by hydrous eclogite when heat flows of 70 mW/m^2 are considered (Figure 9a). At least 0.07 wt.% H_2O and at most 0.3 wt.% H_2O in omphacite are required to explain the lower ($\sim 10^{-2.2}$ S/m) and upper ($\sim 10^{-0.5}$ S/m) bounds, respectively, which corresponds to 0.031–0.053 wt.% H_2O in eclogite. This possibility is further supported by the fact that omphacite with water content as high as or even much more than 0.07 wt.% is frequently observed in these regions (Xia et al., 2005; Katayama et al., 2006; Shen et al., 2007).

Similarly, hydrogen-bearing omphacite can also account for the high conductivity anomalies beneath the Tibetan Plateau (Figure 9b). Guo et al. (2014) claimed that high conductive region higher than $10^{-1.5}$ S/m beneath Tibet cannot be explained by hydrous eclogite, which was based on the low water content in their omphacite (0.032 wt.%). Electrical conductivities calculated in our present model assuming the same water content in omphacite is also just below $10^{-1.5}$ S/m (the lower bound of conductivity anomaly layer) (the *solid black line* in Figure 9b), which is consistent with theirs. So, the key question to decipher the discrepancy is whether or not eclogite can contain omphacite with more than 0.032 wt.% water in this region. It is possible that omphacite suffered from considerable water loss in their eclogite if water content in the coexisting garnet is not altered since water partitioning coefficient in eclogite is expected to be as high as $D^{\text{Omp/Grt}} \approx 5$ – 10 (Katayama et al., 2006; Sheng et al., 2007). If this is the case, it is not necessary to invoke other mechanisms when omphacite at that depth retains its original water content. However, when low heat flow of 50 mW/m^2 is considered, the calculated conductivities are $\sim 10^{-5}$ S/m beneath the Dabie-Sulu UHPM belts (Figure 9c) and $\sim 10^{-2}$ S/m beneath Tibet (Figure 9d), which are much lower than those of geophysical observations (Bai et al., 2010; Wei et al., 2001; Xiao et al., 2007; Xu et al., 2016). Obviously in the case of low surface heat flux, hydrous eclogite is unable to account for the high conductivity anomalies revealed by MT observations beneath the Dabie-Sulu UHPM belts (Figure 9c) and the Tibetan Plateau (Figure 9d). On the contrary, to interpret the conductivity of $\sim 10^{-2.2}$ – $10^{-0.5}$ S/m observed at depths of 10–40 km beneath the Dabie-Sulu UHPM belts of eastern China (Xiao et al., 2007; Xu et al., 2016), the water content of over 7,000 wt. ppm H_2O is required according to Figure 9c. Such water content exceeds the maximum water solubility in omphacite at shallow depth. In fact, the experimental work revealed that water solubility in omphacite is 3,020 wt. ppm H_2O (Katayama & Nakashima, 2003).

Unlike continental collision mentioned above, much deeper high conductivity anomalies associated with oceanic collision, for example, at depths of 250 km at NE Japan (Toh et al., 2006) and at depths of 250–300 km beneath the North Philippine Sea (Tada et al., 2014), cannot be explained by hydrous eclogite. Because of clinopyroxene as the dominant mineral phase, the water storage ability of NAMs in eclogite is the greatest (0.4–0.5 wt.% H_2O) at 2–4 GPa. When pressure exceeds 3 GPa, its H_2O storage capacity gradually decreases from 100 to 410 km since pyroxene progressively dissolves into garnet (Akashi et al., 2009). Instead, the conductivity anomalies may be attributed to fluids released by dehydration of hydrous minerals such as lawsonite (Manthilake et al., 2015) and phengite (Chen et al., 2018).

The eclogite has been considered as one of the important materials for recycling water into the deep mantle (e.g., Katayama et al., 2003, 2006; Katayama & Nakashima, 2003; Liu et al., 2019; Sheng et al., 2007; Xia et al., 2005; Zheng et al., 2016). Study on the diamond-bearing eclogites from the Kokchetav UHPM terrane (Katayama & Nakashima, 2003) revealed that considerable amounts of water can be contained in the NAMs such as omphacite (up to 3,020 wt. ppm H_2O) and garnet (up to 240 wt. ppm H_2O) that sum up to 1,300 wt. ppm water in the bulk rock. Similar water contents were also observed in natural eclogites from the Dabie-Sulu UHPM belts (Sheng et al., 2007; Xia et al., 2005). In the descending oceanic crust, water is incorporated as structurally bound hydroxyl groups in omphacite and garnet in eclogite, which can mostly be transferred to majorite and stishovite at the eclogite-garnetite transition. In such a way, more than 1,000 wt. ppm water can be transported into the mantle transition zone (Katayama et al., 2003). In comparison with the experimental conductivity data (Figure 9), it is suggested that the bulk water contents in the deep-subducted eclogite is no more than 700 wt. ppm. This observation implies that the efficiency of water

cycling by eclogite subduction is not as high as previously thought. Besides the NAMs (i.e., omphacite and garnet) in eclogite, lawsonite or phengite is stable up to a depth of 150–300 km in cold subduction zones (Domanik & Holloway, 1996; Ono, 1998; Schmidt & Poli, 1998), which are also considered as the effective water carriers in the subducted oceanic crust.

5. Conclusions

The present study demonstrates the influence of water and iron content on the electrical conductivity of omphacite and reveals that water enhances the electrical conductivity of omphacite significantly, while iron serves as an effective assistant to make hydrogen move easier and faster and therefore result in smaller activation enthalpy and higher conductivity. The laboratory-based conductivity-depth profiles were calculated using the present conductivity data combined with conductivity of garnet and petrological models. The conductivity-depth profiles suggest that geophysically observed high conductivity anomalies beneath the Dabie-Sulu UHPM belts and the Tibetan Plateau could be attributed to the presence of hydrous eclogite (0.07 wt.% H₂O) if relatively high heat flow (70 mW/m²) is assumed. However, when a lower heat flow (50 mW/m²) is considered, other mechanisms are required.

Acknowledgments

The authors appreciate the anonymous Associate Editor, Kiyoshi Fuji-ta, and three anonymous reviewers for their constructive comments that greatly improved the manuscript. We would like to thank Chao Liu for XRD analysis, and Daisuke Yamazaki, Akira Yoneda, and Eiji Ito for their suggestions and discussions. This study was financially supported by the Foundation of School of Earth Sciences, Zhejiang University, Key Research Program of Frontier Sciences of CAS (ZDBS-LY-DQC015), NSF of China (41973056, 41773056, and 41303048), Science Foundation of Guizhou Province (2017-1196 and 2018-1176) to B. Z., and JSPS MEXT/KAKENHI (Grants JP15H05827 and 17H01155) to T. Y. This study was performed using joint-use facilities of IPM, Okayama University. The authors comply with AGU's data policy; all data supporting the conclusions of this paper are available in Figshare (https://figshare.com/articles/Zhang_et_al_JGR_2019_xls/10911911). The authors declare no competing financial interests.

References

- Akashi, A., Nishihara, Y., Takahashi, E., Nakajima, Y., Tange, Y., & Funakoshi, K. I. (2009). Orthoenstatite/clinoenstatite phase transformation in MgSiO₃ at high-pressure and high-temperature determined by in situ X-ray diffraction: Implications for nature of the X discontinuity. *Journal of Geophysical Research*, *114*, B04206. <https://doi.org/10.1029/2008JB005894>
- Anderson, D. L. (2005). Large igneous provinces, delamination, and fertile mantle. *Elements*, *1*(5), 271–275. <https://doi.org/10.2113/gselements.1.5.271>
- Bagdassarov, N., Batalev, V., & Egorova, V. (2011). State of lithosphere beneath Tien Shan from petrology and electrical conductivity of xenoliths. *Journal of Geophysical Research*, *116*, B01202. <https://doi.org/10.1029/2009JB007125>
- Bai, D., Unsworth, M. J., Meju, M. A., Ma, X., Teng, J. W., Kong, X. R., et al. (2010). Crustal deformation of the eastern Tibetan plateau revealed by magnetotelluric imaging. *Nature Geoscience*, *3*(5), 358–362. <https://doi.org/10.1038/ngeo830>
- Chen, S., Guo, X., Yoshino, T., Jin, Z., & Li, P. (2018). Dehydration of phengite inferred by electrical conductivity measurements: Implication for the high conductivity anomalies relevant to the subduction zones. *Geology*, *46*(1), 11–14. <https://doi.org/10.1130/G39716.1>
- Dai, L., Hu, H., Li, H., Wu, L., Hui, K., Jiang, J., & Sun, W. (2016). Influence of temperature, pressure, and oxygen fugacity on the electrical conductivity of dry eclogite, and geophysical implications. *Geochemistry, Geophysics, Geosystems*, *17*, 2394–2407. <https://doi.org/10.1002/2016GC006282>
- Domanik, K. J., & Holloway, J. R. (1996). The stability and composition of phengitic muscovite and associated phases from 5.5 to 11 GPa: Implications for deeply subducted sediments. *Geochimica Cosmochimica Acta*, *60*, 4133–4150. [https://doi.org/10.1016/S0016-7037\(96\)00241-4](https://doi.org/10.1016/S0016-7037(96)00241-4)
- Frost, B. R., Fyfe, W. S., Tazaki, K., & Chan, T. (1989). Grain-boundary graphite in rocks and implications for high electrical conductivity in the lower crust. *Nature*, *340*(6229), 134–136. <https://doi.org/10.1038/340134a0>
- Frost, D. J., & McCammon, C. A. (2008). The redox state of Earth's mantle. *Annual Review of Earth and Planetary Sciences*, *36*, 389–420. <https://doi.org/10.1146/annurev.earth.36.031207.124322>
- Fuji-ta, K., Katsura, T., & Tainosho, Y. (2004). Electrical conductivity measurement of granulite under mid-to lower crustal pressure-temperature conditions. *Geophysical Journal International*, *157*(1), 79–86. <https://doi.org/10.1111/j.1365-246X.2004.02165.x>
- Glover, P. W. J. (1996). Graphite and electrical conductivity in the lower continental crust: A review. *Physics and Chemistry of the Earth*, *21*(4), 279–287. [https://doi.org/10.1016/S0079-1946\(97\)00049-9](https://doi.org/10.1016/S0079-1946(97)00049-9)
- Guo, Y., Wang, D., Shi, Y., Zhou, Y., Dong, Y., & Li, C. (2014). The electrical conductivity of eclogite in Tibet and its geophysical implications. *Science China. Earth Sciences*, *57*(9), 2071–2078. <https://doi.org/10.1007/s11430-014-4876-6>
- Hacker, B. R., Gnos, E., Ratschbacher, L., Grove, M., McWilliams, M., Sobolev, S. V., et al. (2000). Hot and dry deep crustal xenoliths from Tibet. *Science*, *287*(5462), 2463–2466. <https://doi.org/10.1126/science.287.5462.2463>
- Hu, S., He, L., & Wang, J. (2000). Heat flow in the continental area of China: A new data set. *Earth and Planetary Science Letters*, *179*(2), 407–419. [https://doi.org/10.1016/S0012-821X\(00\)00126-6](https://doi.org/10.1016/S0012-821X(00)00126-6)
- Huebner, J. S., & Voigt, D. E. (1988). Electrical conductivity of diopside; evidence for oxygen vacancies. *American Mineralogist*, *73*(11–12), 1235–1254.
- Irfune, T., Sekine, T., Ringwood, A., & Hibberson, W. (1986). The eclogite–garnetite transformation at high pressure and some geophysical implications. *Earth and Planetary Science Letters*, *77*(2), 245–256. [https://doi.org/10.1016/0012-821X\(86\)90165-2](https://doi.org/10.1016/0012-821X(86)90165-2)
- Katayama, I., Hirose, K., Yurimoto, H., & Nakashima, S. (2003). Water solubility in majoritic garnet in subducting oceanic crust. *Geophysical Research Letters*, *30*(22), 2155. <https://doi.org/10.1029/2003GL018127>
- Katayama, I., & Nakashima, S. (2003). Hydroxyl in clinopyroxene from the deep subducted crust: Evidence for H₂O transport into the mantle. *American Mineralogist*, *88*(1), 229–234. <https://doi.org/10.2138/am-2003-0126>
- Katayama, I., Nakashima, S., & Yurimoto, H. (2006). Water content in natural eclogite and implication for water transport into the deep upper mantle. *Lithos*, *86*(3–4), 245–259. <https://doi.org/10.1016/j.lithos.2005.06.006>
- Koch-Müller, M., Matsuyuk, S. S., & Wirth, R. (2004). Hydroxyl in omphacites and omphacitic clinopyroxenes of upper mantle to lower crustal origin beneath the Siberian platform. *American Mineralogist*, *89*(7), 921–931. <https://doi.org/10.2138/am-2004-0701>
- Landauer, R. (1952). The electrical resistance of binary metallic mixtures. *Journal of Applied Physics*, *23*(7), 779–784. <https://doi.org/10.1063/1.1702301>
- Laštovičková, M., & Parchomenko, E. I. (1976). The electric properties of eclogites from the Bohemian Massif under high temperatures and pressures. *Pure and Applied Geophysics*, *114*(3), 451–460. <https://doi.org/10.1007/BF00876944>

- Liu, H., Zhu, Q., & Yang, X. (2019). Electrical conductivity of OH-bearing omphacite and garnet in eclogite: The quantitative dependence on water content. *Contributions to Mineralogy and Petrology*, *174*(7), 57. <https://doi.org/10.1007/s00410-019-1593-3>
- Manthilake, G., Mookherjee, M., Bolfan-Casanova, N., & Andrault, D. (2015). Electrical conductivity of lawsonite and dehydrating fluids at high pressures and temperatures. *Geophysical Research Letters*, *42*, 7398–7405. <https://doi.org/10.1002/2015GL064804>
- Miao, S., Li, H., & Chen, G. (2014). The temperature dependence of thermal conductivity for lherzolites from the North China Craton and the associated constraints on the thermodynamic thickness of the lithosphere. *Geophysical Journal International*, *197*, 900–909. <https://doi.org/10.1093/gji/ggu020>
- Mooney, W. D., & Kaban, M. K. (2010). The North American upper mantle: Density, composition, and evolution. *Journal of Geophysical Research*, *115*, B12424. <https://doi.org/10.1029/2010JB000866>
- Naif, S., Key, K., Constable, S., & Evans, R. L. (2013). Melt-rich channel observed at the lithosphere-asthenosphere boundary. *Nature*, *495*(7441), 356–359. <https://doi.org/10.1038/nature11939>
- Omura, K., Kurita, K., & Kumazawa, M. (1989). Experimental study of pressure dependence of electrical conductivity of olivine at high temperatures. *Physics of the Earth and Planetary Interiors*, *57*(3-4), 291–303. [https://doi.org/10.1016/0031-9201\(89\)90118-0](https://doi.org/10.1016/0031-9201(89)90118-0)
- Ono, S. (1998). Stability limits of hydrous minerals in sediment and mid-ocean ridge basalt compositions: Implications for water transport in subduction zones. *Journal of Geophysical Research*, *103*, 18,253–18,267. <https://doi.org/10.1029/98JB01351>
- Paterson, M. S. (1982). The determination of hydroxyl by infrared absorption in quartz, silicate glasses and similar materials. *Bulletin de Mineralogie*, *105*, 20–29.
- Poe, B. T., Romano, C., Nestola, F., & Smyth, J. R. (2010). Electrical conductivity anisotropy of dry and hydrous olivine at 8 GPa. *Physics of the Earth and Planetary Interiors*, *181*(3-4), 103–111. <https://doi.org/10.1016/j.pepi.2010.05.003>
- Reynard, B., Mibe, K., & Van de Moortèle, B. (2011). Electrical conductivity of the serpentinised mantle and fluid flow in subduction zones. *Earth and Planetary Science Letters*, *307*(3-4), 387–394. <https://doi.org/10.1016/j.epsl.2011.05.013>
- Schmidt, M. W., & Poli, S. (1998). Experimentally based water budgets for dehydrating slabs and consequences for arc magma generation. *Earth and Planetary Science Letters*, *163*, 361–379. [https://doi.org/10.1016/S0012-821X\(98\)00142-3](https://doi.org/10.1016/S0012-821X(98)00142-3)
- Sheng, Y. M., Xia, Q. K., Dallai, L., Yang, X. Z., & Hao, Y. T. (2007). H₂O contents and D/H ratios of nominally anhydrous minerals from ultrahigh-pressure eclogites of the Dabie orogen, eastern China. *Geochimica et Cosmochimica Acta*, *71*(8), 2079–2103. <https://doi.org/10.1016/j.gca.2007.01.018>
- Smyth, J. R., Bell, D. R., & Rossman, G. R. (1991). Incorporation of hydroxyl in upper-mantle clinopyroxenes. *Nature*, *351*(6329), 732–735. <https://doi.org/10.1038/351732a0>
- Tada, N., Baba, K., & Utada, H. (2014). Three-dimensional inversion of seafloor magnetotelluric data collected in the Philippine Sea and the western margin of the northwest Pacific Ocean. *Geochemistry, Geophysics, Geosystems*, *15*, 2895–2917. <https://doi.org/10.1002/2014GC005421>
- Toh, H., Baba, K., Ichiki, M., Motobayashi, T., Ogawa, Y., Mishina, M., & Takahashi, I. (2006). Two-dimensional electrical section beneath the eastern margin of Japan Sea. *Geophysical Research Letters*, *33*, L22309. <https://doi.org/10.1029/2006GL027435>
- Wang, D., Karato, S., & Jiang, Z. (2013). An experimental study of the influence of graphite on the electrical conductivity of olivine aggregates. *Geophysical Research Letters*, *40*, 2028–2032. <https://doi.org/10.1002/grl.50471>
- Wang, Z., Ji, S., & Dresen, G. (1999). Hydrogen-enhanced electrical conductivity of diopside crystals. *Geophysical Research Letters*, *26*(6), 799–802. <https://doi.org/10.1029/1999GL900094>
- Wei, W., Unsworth, M., Jones, A., Booker, J., Tan, H. D., Nelson, D., et al. (2001). Detection of widespread fluids in the Tibetan crust by magnetotelluric studies. *Science*, *292*(5517), 716–718. <https://doi.org/10.1126/science.1010580>
- Xia, Q. K., Chen, D., Carpenter, S., Zhi, X., Wang, R., & Cheng, H. (2000). Hydrogen diffusion in clinopyroxene: Dehydration experiments. *Science in China Series D: Earth Sciences*, *43*(6), 561–568. <https://doi.org/10.1007/BF02879499>
- Xia, Q. K., Sheng, Y. M., Yang, X. Z., & Yu, H. M. (2005). Heterogeneity of water in garnets from UHP eclogites, eastern Dabieshan, China. *Chemical Geology*, *224*(4), 237–246. <https://doi.org/10.1016/j.chemgeo.2005.08.003>
- Xiao, Q. B., Zhao, G. Z., Zhan, Y., Chen, X. B., Tang, J., Wang, J. J., & Deng, Q. H. (2007). A preliminary study on electrical structure and dynamics of the ultrahigh pressure metamorphic belt beneath the Dabie Mountains. *Chinese Journal of Geophysics*, *50*(3), 710–721. <https://doi.org/10.1002/cjg2.1085>
- Xu, J., Zhang, D., Fan, D., Dera, P. K., Shi, F., & Zhou, W. (2019). Thermoelastic properties of eclogitic garnets and omphacites: Implications for deep subduction of oceanic crust and density anomalies in the upper mantle. *Geophysical Research Letters*, *46*, 179–188. <https://doi.org/10.1029/2018GL081170>
- Xu, Y., Zhang, S., Griffin, W. L., Yang, Y., Yang, B., Luo, Y., et al. (2016). How did the Dabie Orogen collapse? Insights from 3-D magnetotelluric imaging of profile data. *Journal of Geophysical Research: Solid Earth*, *121*, 5169–5185. <https://doi.org/10.1002/2015JB012717>
- Yang, X. (2012). Orientation-related electrical conductivity of hydrous olivine, clinopyroxene and plagioclase and implications for the structure of the lower continental crust and uppermost mantle. *Earth and Planetary Science Letters*, *317*, 241–250. <https://doi.org/10.1016/j.epsl.2011.11.011>
- Yang, X., & Heidelbach, F. (2012). Grain size effect on the electrical conductivity of clinopyroxene. *Contributions to Mineralogy and Petrology*, *163*(6), 939–947. <https://doi.org/10.1007/s00410-011-0707-3>
- Yang, X., Keppler, H., McCammon, C., Ni, H., Xia, Q., & Fan, Q. (2011). Effect of water on the electrical conductivity of lower crustal clinopyroxene. *Journal of Geophysical Research*, *116*, B04208. <https://doi.org/10.1029/2010JB008010>
- Yang, X., & McCammon, C. (2012). Fe³⁺-rich augite and high electrical conductivity in the deep lithosphere. *Geology*, *40*(2), 131–134. <https://doi.org/10.1130/G32725.1>
- Yoshino, T. (2010). Laboratory electrical conductivity measurement of mantle minerals. *Surveys in Geophysics*, *31*(2), 163–206. <https://doi.org/10.1007/s10712-009-9084-0>
- Yoshino, T., & Katsura, T. (2009). Effect of iron content on electrical conductivity of ringwoodite, with implications for electrical structure in the mantle transition zone. *Physics of the Earth and Planetary Interiors*, *174*(1-4), 3–9. <https://doi.org/10.1016/j.pepi.2008.09.015>
- Yoshino, T., Matsuzaki, T., Yamashita, S., & Katsura, T. (2006). Hydrous olivine unable to account for conductivity anomaly at the top of the asthenosphere. *Nature*, *443*(7114), 973–976. <https://doi.org/10.1038/nature05223>
- Yoshino, T., & Noritake, F. (2011). Unstable graphite films on grain boundaries in crustal rocks. *Earth and Planetary Science Letters*, *306*(3-4), 186–192. <https://doi.org/10.1016/j.epsl.2011.04.003>
- Yoshino, T., Shimozuku, A., Shan, S., Guo, X., Yamazaki, D., Ito, E., et al. (2012). Effect of temperature, pressure and iron content on the electrical conductivity of olivine and its high-pressure polymorphs. *Journal of Geophysical Research*, *117*, B08205. <https://doi.org/10.1029/2011JB008774>

- Zhang, B. H., & Yoshino, T. (2016). Effect of temperature, pressure and iron content on the electrical conductivity of orthopyroxene. *Contributions to Mineralogy and Petrology*, *171*(12), 102. <https://doi.org/10.1007/s00410-016-1315-z>
- Zhang, B. H., & Yoshino, T. (2017). Effect of graphite on the electrical conductivity of the lithospheric mantle. *Geochemistry, Geophysics, Geosystems*, *18*, 23–40. <https://doi.org/10.1002/2016GC006530>
- Zhang, B. H., Yoshino, T., Wu, X. P., Matsuzaki, T., Shan, S., & Katsura, T. (2012). Electrical conductivity of enstatite as a function of water content: Implications for the electrical structure in the upper mantle. *Earth and Planetary Science Letters*, *357–358*, 11–20. <https://doi.org/10.1016/j.epsl.2012.09.020>
- Zhang, B. H., Yoshino, T., Yamazaki, D., Manthilake, G., & Katsura, T. (2014). Electrical conductivity anisotropy in partially molten peridotite under shear deformation. *Earth and Planetary Science Letters*, *405*, 98–109. <https://doi.org/10.1016/j.epsl.2014.08.018>
- Zhao, C., & Yoshino, T. (2016). Electrical conductivity of mantle clinopyroxene as a function of water content and its implication on electrical structure of uppermost mantle. *Earth and Planetary Science Letters*, *447*, 1–9. <https://doi.org/10.1016/j.epsl.2016.04.028>
- Zheng, Y., Chen, R., Xu, Z., & Zhang, S. (2016). The transport of water in subduction zones. *Science China Earth Sciences*, *59*(4), 651–682. <https://doi.org/10.1007/s11430-015-5258-4>